ORIGINAL ARTICLE

Computational fluid dynamics model for thickness and uniformity prediction of coating layer in slot-die process

Seongyong Kim[1] · Jongsu Lee[1] · Changwoo Lee[2]

Abstract
A three-dimensional computational fluid dynamics model to analyze the dynamics of ink at the outlet of a slot-die coater and wet coated layer thickness is presented in this paper. This model can be used to estimate the thickness deviation of the coated layer in the transverse direction, which cannot be obtained by using the conventional two-dimensional model. The internal geometry of the slot-die coater was statistically optimized by using the Box–Behnken design of experiment. Experimental results show that the thickness deviation is improved by 71% in the slot-die coater having an optimal internal geometry and inlet flow rate. The developed model is expected to be useful in obtaining the desired coating conditions and geometry of the slot-die coater without costly and time-consuming experiments.

Keywords Roll-to-roll · Slot-die coating · Computational fluid dynamics · Design of experiments

1 Introduction

Printed electronic devices have been spotlighted as a next-generation electronics field [1–4]. In the field of printed photovoltaics and batteries, the level of device manufacturing technique is reaching close to making commercialization feasible. Conventional paper-based printing techniques, such as gravure, screen, inkjet printing, and slot-die coating, have been used to print functional layers for fabrication of the printed electronic devices. Particularly, the slot-die coating is widely used because of its characteristics of large-area coating and easy control of the coated layer thickness [5, 6]. Thus far, many studies have been reported on the dynamics of ink in the

slot-die coating, statistical optimization of the coating process, and its application. Scriven et al. determined the low limit of wet coated layer thickness considering a viscocapillary model [7]. Lee et al. proposed a fluid model to form a thin film in the slot-die coating followed by verification of the model using the flow network modeling method [8]. Romero et al. analyzed the dynamics of ink in the ink deposition phase using computational fluid dynamics (CFD) [9–12]. Park et al. statistically optimized the slot-die coating conditions using a response surface methodology in an antireflection film coating [12]. Lee et al. analyzed the relation between the tension, velocity, and ink viscosity on the thickness and roughness of printed patterns using the two-level full-factorial design of experiments [13]. Based on the analyses, a transparent conductive layer [14–16], photovoltaics [17–20], and organic light-emitting diodes [21] can be fabricated using various functional inks, such as graphene and silver nanowires. In most previous studies, the dynamics of the ink in the coating process were analyzed under the assumption that the thickness of the coated layer is uniform in the transverse direction. However, the ink velocity at the outlet of the slot-die coater could be different in the transverse direction according to the geometry of the slot-die coater and coating conditions, resulting in various coating defects. In this study, the dynamics of ink at the outlet of the slot-die coater were analyzed using three-dimensional CFD models. The geometry of the slot-die coater was optimized using a Box–Behnken

✉ Changwoo Lee
   changwoo1220@icloud.com

   Seongyong Kim
   arsen6788@gmail.com

   Jongsu Lee
   ljs8755@gmail.com

1 Department of Mechanical Design and Production Engineering, Konkuk University, 120, Neungdong-ro, Gwangjin-gu, Seoul 05029, South Korea

2 Department of Mechanical Engineering, Konkuk University, 120, Neungdong-ro, Gwangjin-gu, Seoul 05029, South Korea

experimental design, which is a representative statistical optimization technique, followed by experimental verifications.

2 Thickness estimation of the coated layer using CFD

Figure 1 presents the schematics of the slot-die coater. In the figure, ink is filled in the reservoir of the slot-die coater by an ink supplier and coated on a substrate through the shim plate. The velocity of ink at the outlet of the coater can be changed according to the geometry of the reservoir, resulting in the thickness variation of the coated layer.

2.1 Modeling of dynamics of ink in the slot-die coater using CFD

The dynamics of ink in the slot-die coater were modeled using a CFD technique (ABAQUS V6.14) to analyze the velocity difference of ink according to the geometry of the slot-die coater in the transverse direction. Equation (1) presents the governing equation of the dynamics of ink in the inner side of the slot-die coater. Equation (1) represents the Navier–Stokes equation for an incompressible fluid and the Reynolds number of the fluid is approximately 122; therefore, the flow was set to laminar flow. With respect to the boundary conditions, the flow rate, pressure, and wall conditions were set to those at the inlet, outlet, and side of the flow model, respectively. The flow rate was set to 1~30 mm/s at the inlet, and the pressure was set to 101,325 Pa at the outlet.

$$\frac{d}{dt}\int_v \rho v dV + \int_s \rho v \otimes (v - v_m) \cdot \varphi d\Gamma$$
$$= \int_v \nabla p dV + \int_s \tau \cdot \varphi d\Gamma + \int_v f dV \qquad (1)$$

where V is an arbitrary control volume having surface Γ, φ is the normal vector on Γ, ρ is the fluid density, p is pressure, v is a velocity vector, v_m is the velocity of the moving elements, f is the body force, and τ is the viscous shear stress.

Flow resistance in the viscous fluid can be derived by the relation between a derivative stress applied to elements and strain rate, as shown in Eq. (2).

$$\sigma = 2\eta \dot{e} = \eta \dot{\gamma} \qquad (2)$$

where σ is the derivative stress, $\dot{e}$ is the strain rate of the element to which σ is applied, η is the viscosity of the fluid, and $\dot{\gamma}$ is the nominal shear strain.

Table 1 presents the properties of the ink and coating conditions. Considering the ink used in this study, a gadolinium-doped ceria (GDC), which is a ceramic electrolyte in a solid oxide fuel cell, fluid type, was set to the Newtonian fluid. The density and viscosity of the ink were 3.4 g/cm³ and 100 cP, respectively. The pressure in the output of the slot-die coater was atmospheric pressure. Figure 2 presents the internal geometries of the slot-die coater considered in this study. The factors affecting the slot-die coater outlet speed were selected as the design parameters in the optimization. The levels of each factor were determined considering the range of the factor used in the actual process. The reservoir angle was 25°, thickness of the shim plate was 120 μm, and flow rate was 10 mm/s. The width of the coating layer was 0.1 m, and the film speed was 1 m/min. The number of coated strips was 1. Figure 3 presents the velocity profile of the ink at the outlet of the slot-die coater in the transverse direction. The velocity profiles were derived from the velocity at the outlet of the slot-die coater using the CFD simulation. Using the derived velocity distribution, the wet thickness of the coated layer was estimated using the model in Section 2.2.

2.2 Wet thickness estimation model

The wet thickness of the coated layer according to the velocity of the coated ink at the outlet of the coater can be easily

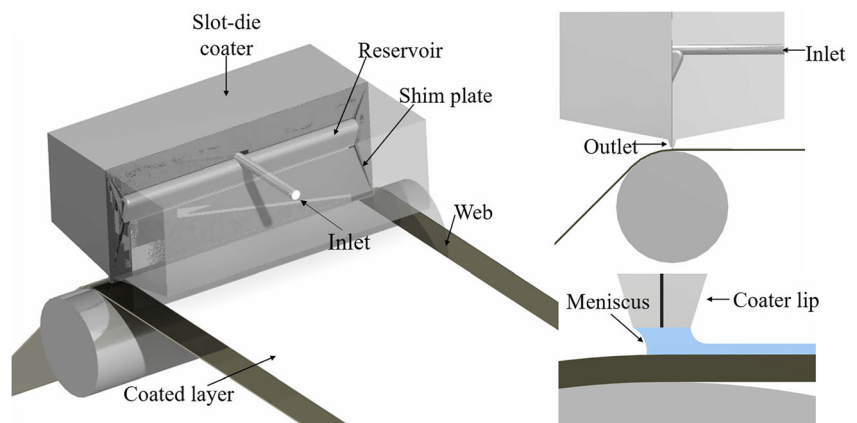
Fig. 1 Schematics of the slot-die coater

Table 1 Properties of yttria-stabilized zirconia and coating conditions

Parameter	Units	Value
Fluid type	–	Newtonian
Outlet pressure	Pa	101,325
Fluid viscosity	cP	100
Fluid density	g/cm^2	3.4
Coated layer width	m	0.1
Film speed	m/min	1

obtained by the mass conservation law in the control volume, marked in Fig. 1.

$$\frac{d}{dt}\int C(x)dx = f_r - [NwtS] \tag{3}$$

where x is a coating direction, i.e., film transported direction, $C(x)$ is the volume of the coated layer according to x, f_r is the flow rate of the coated ink, N is the number of strips of the coated layer, t is the wet thickness of the coated layer, w is the width of the unit strip, t is the thickness of the coated layer, and S is the film transported speed.

In the steady state, Eq. (3) can be simplified as follows:
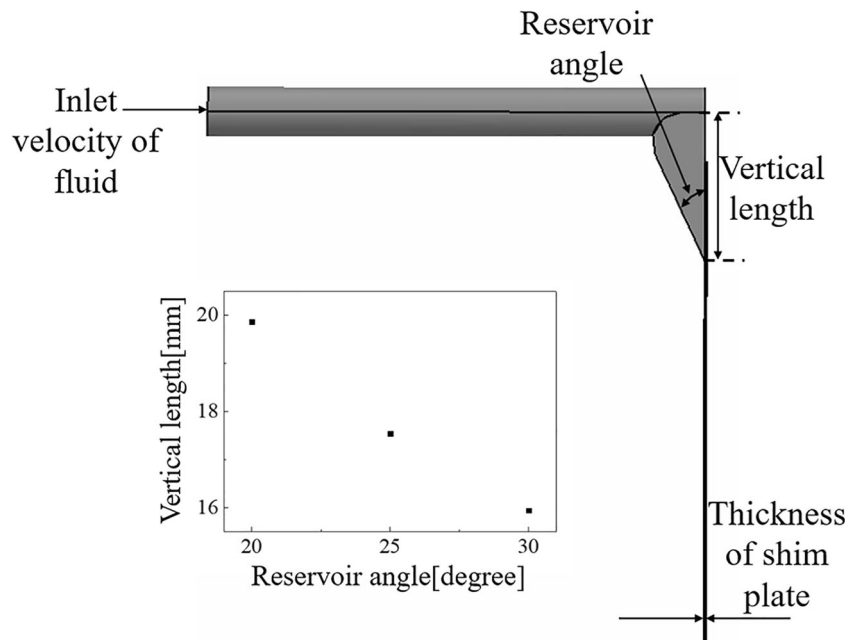
$$f_r = nwtS \tag{4}$$

In Eq. (4), t can be obtained as shown in Eq. (5). If the number of strips is 1, Eq. (5) can be simplified as Eq. (6).

$$t = \frac{f_r}{NwS} \tag{5}$$

$$t = \frac{f_r}{wS} \tag{6}$$

In Eq. (6), a widening after coating is not considered. However, the widening or ink agglomeration could be generated by the difference between the surface tension of the ink and surface energy of the substrate. The thickness variation can be considered by applying a correction factor K to the numerator of Eq. (6): K can be obtained empirically [22]. In this study, K was determined as 0.3.

2.3 Experimental verifications

Figure 4 presents the roll-to-roll slot-die coating system (a) and the slot-die coater (b). Figure 5 presents the estimated coating thickness derived by the CFD model and the wet thickness estimation model in Section 2. In Fig. 5, black rectangular marks and red circular marks present the coating layer thickness estimated by the CFD and wet thickness estimation model and the measured thickness of the coated layer, respectively. One can see that the trend of the estimated thickness is similar to that of the measured thickness. To evaluate the estimation ability of the proposed models, a normalized root mean square deviation (NRMSD), shown in Eq. (7), was used.

$$\mathrm{NRMSD} = \frac{\sqrt{\frac{\sum_{t=1}^{n}\left(T_t - \hat{T}_t\right)^2}{n}}}{T_{\max} - T_{\min}} \tag{7}$$

where $T_{\max}$ and $T_{\min}$ are the maximum and minimum values in the measured thickness data, respectively; T_t and $\hat{T}_t$ are the measured and estimated thickness at tth data point, respectively; and n is the number of data points for NRMSD.

For experimental verification, the internal angle of the reservoir was set to 25°, the flow rate was set to 10 mm/s, and the
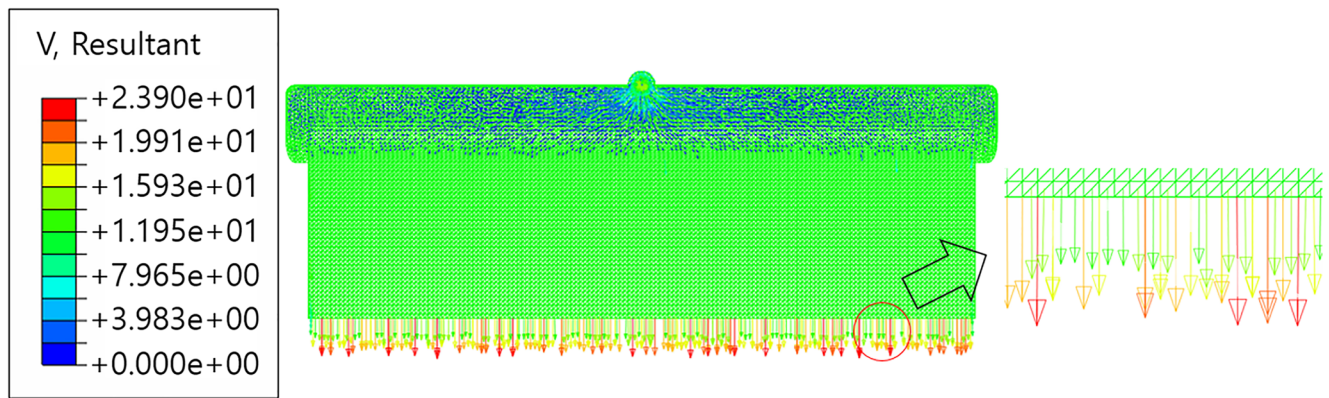
Fig. 2 Internal geometry of the slot-die coater used in this study

Fig. 3 Velocity profile of the discharged ink at the outlet of the slot-die coater in the transverse direction

shim plate thickness was 120 μm. The average measured and estimated coated layer thicknesses are approximately 14.18 and 14.86 μm, respectively. The estimated model has a 92.3% estimation ability. Using the proposed models, the input flow rate and internal geometry of the slot-die coater were statistically optimized using the Box–Behnken experimental design.

3 Optimization of the internal geometry of the slot-die coater

The internal geometry of the slot-die coater, i.e., the reservoir angle and thickness of the shim plate, and the input flow rate were statistically optimized to improve the uniformity of the velocity profile of ink in the transverse direction at the output of the slot-die coater. The range of the reservoir angles was 25° (− 1) to 35° (1). The volume of the reservoir section in which the supplied ink from the inlet was filled could be different according to the reservoir angle. The vertical length shown in Fig. 3 was determined according to the reservoir angle (shown in the inner figure of Fig. 3) to maintain the reservoir volume consistently. The range of the shim plate

thicknesses was determined from 120 (− 1) to 160 μm (1) considering the shim plate thickness used in previous research [12]. The inlet flow rates were determined to 1 (− 1), 10 (0) and 30 ml/min (1).The GDC was coated according to the experimental order design by the Box–Behnken model shown in Table. 2. The output velocity deviation according to the factors was evaluated by the standard deviation of the obtained velocity profile to the average velocity of the profile, as shown in Eq. (8). The right-end column in Table 2 presents the thickness deviation of the coated layer according to the internal geometries of the slot-die coater and inlet flow rate.

$$
u = \frac{\sqrt{\dfrac{\sum\limits_{i=1}^{n} \left(a_i - \overline{a}\right)^2}{n-1}}}{\dfrac{1}{n} \sum\limits_{i=1}^{n} a_i}
\tag{8}
$$

where u is standard deviation of velocity profile in the width direction; n is the number of calculated points in a velocity profile; and a_i is the velocity of the nth point in the velocity profile.

Analysis of variance (ANOVA) was used to determine the statistical significance of the three factors. The
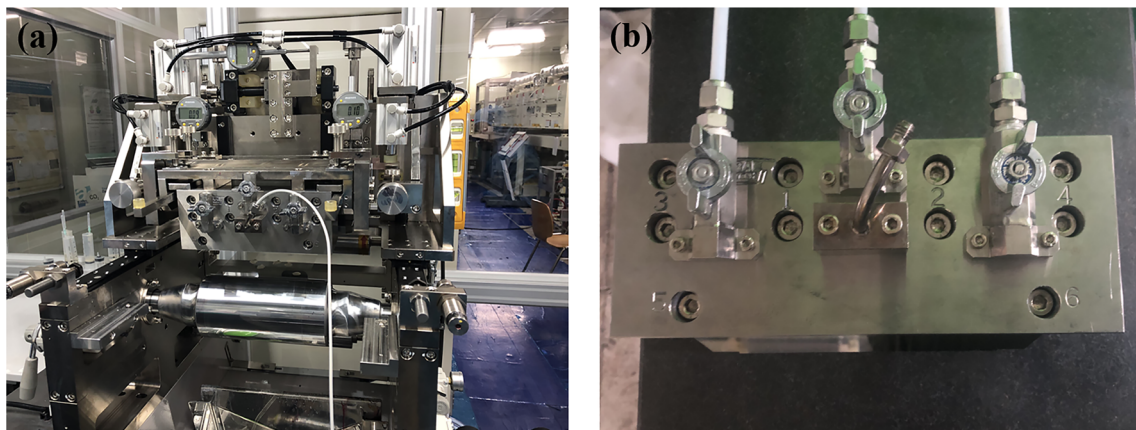

Fig. 4 **a** Roll-to-roll slot-die coating system and **b** the slot-die coater
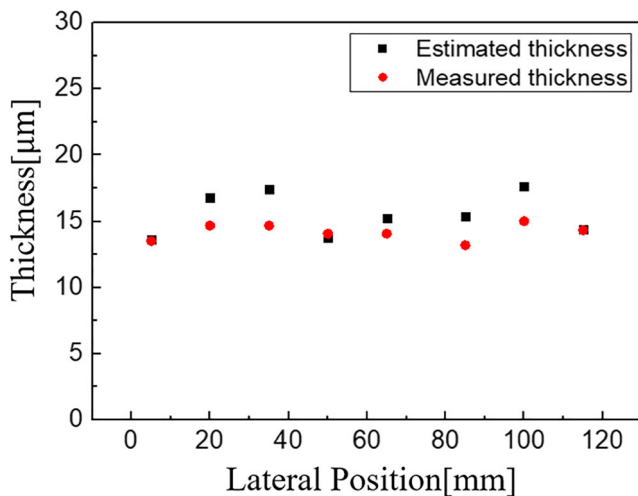
Fig. 5 Estimated coated layer thickness derived by using the CFD model and the wet thickness estimation model in Section 2, and the measured coated layer thickness

Fig. 6 Pareto chart

significance of the three factors was evaluated with the help of a Pareto chart, which is a useful tool to express the significant level graphically, as shown in Fig. 6. In the figure, the x- and y-axes are the standardized significance and the main and interaction effects of the factors. "A," "B," and "C" are the shim plate thickness, inlet flow rate, and reservoir angle, respectively, on the y-axis. The red-dotted line is the criterion of the significant evaluation. In the statistical analysis results, the standardized significant at a confidence interval of 95% is 0.0988, and if a factor has a standardized significant larger than 0.0988, the factor is considered to be significant on the thickness variation at the 95% confidence interval. One can see that the main effect of the reservoir angle affects the thickness deviation most significantly, followed by the main effects
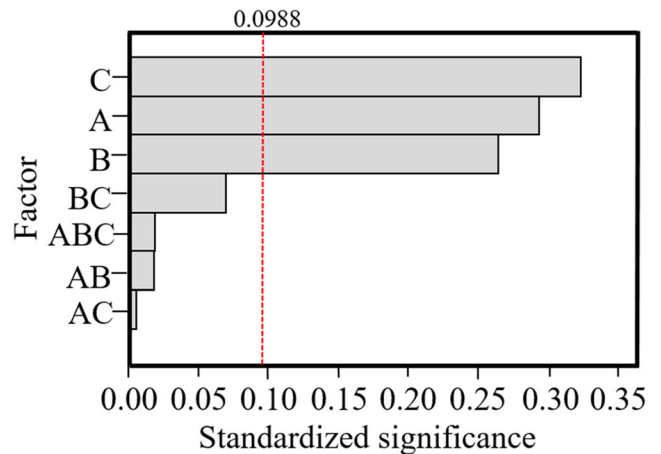
of the shim plate thickness and the inlet flow rate. Using the significant factors, a regression model was obtained as Eq. (9). Thickness deviations according to the factors were calculated using the model, and the optimal level of each factor was determined by using a desirability function, which is one of the most currently used criterion approach in the optimization of input factors [23]. The range of the desirability function is 0 (worst)–1 (best). The measured thickness deviations were transformed into numbers on a dimensionless desirability scale.

$$Th = 0.2271 + 0.00147x_1 + 0.00489x_2 + 0.00122x_3 \quad (9)$$

where x_1, x_2, and x_3 are the normalized levels of the shim plate thickness, reservoir angle, and inlet flow rate, respectively, and Th is the estimated thickness deviation.

Equation (10) presents the minimum desirability function used in this study. In the minimum desirability function, d_m is increased with decreasing y.

Table 2 Experimental order based on thickness deviation and the corresponding results

Run order	Inlet velocity	Thickness of shim plate	Reservoir angle	Thickness deviation
1	1	− 1	0	0.0178
2	0	1	− 1	0.0216
3	− 1	1	0	0.0193
4	1	1	0	0.0210
5	− 1	− 1	0	0.0216
6	0	1	1	0.0213
7	0	− 1	− 1	0.0211
8	1	0	− 1	0.0215
9	0	− 1	1	0.0210
10	1	0	0	0.0227
11	1	0	1	0.0231
12	− 1	0	− 1	0.0223
13	− 1	0	0	0.0242
14	− 1	0	1	0.0241
15	0	0	0	0.0287

$$
d_m = \begin{cases} 1 & if \ y < T \\ \left(\dfrac{y-M}{T-M}\right)^s & if \ T \leq y \leq M \\ 0 & if \ y > M \end{cases} \tag{10}
$$

where d_m is the desirability value; y and T are the measured and target values, respectively; M is the upper permissible value; and exponent s is the weight that shows the importance of the target value. In this study, T, M, and the exponents s were 1.2, 4, and 1, respectively.

Figure 7 presents the d_m of the ideal ($d_m = 1$) and optimal cases, and experimental results shown in Table 2. The d_m values over 0.9, between 0.6 and 0.89, and below 0.59 have good, appropriate, and bad coating qualities [24]. In the optimal case, the inlet flow rate, reservoir angle, and thickness of shim plate are 23 mm/ s (0.65), 25° (− 1) and 120 μm (− 1), and the corresponding d_m is 0.95. The thickness deviation is below 0.0147. The GDC was coated in the optimal levels of the factors to experimentally verify the effects of the determined conditions on the improvement of the thickness deviation. Figure 8 presents the thickness profiles of the wet coated layer before and after the optimization of the factors. In the conventional case, the inlet flow rate, reservoir angle, and shim plate thickness are 10 ml/min (0), 30° (0), and 140 μm (0), respectively, and it has a thickness deviation of 0.0287. It can be seen that the average thickness deviation is decreased by 71%, which demonstrates the effect of optimization.

4 Conclusion

In this study, we developed a three-dimensional slot-die coating model by using the CFD technique to analyze the
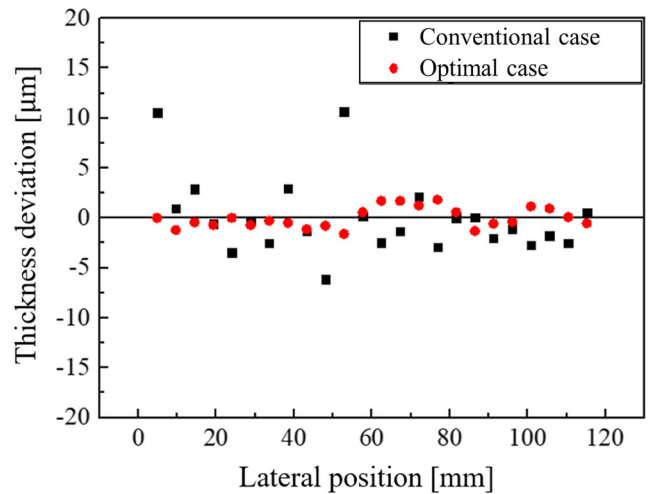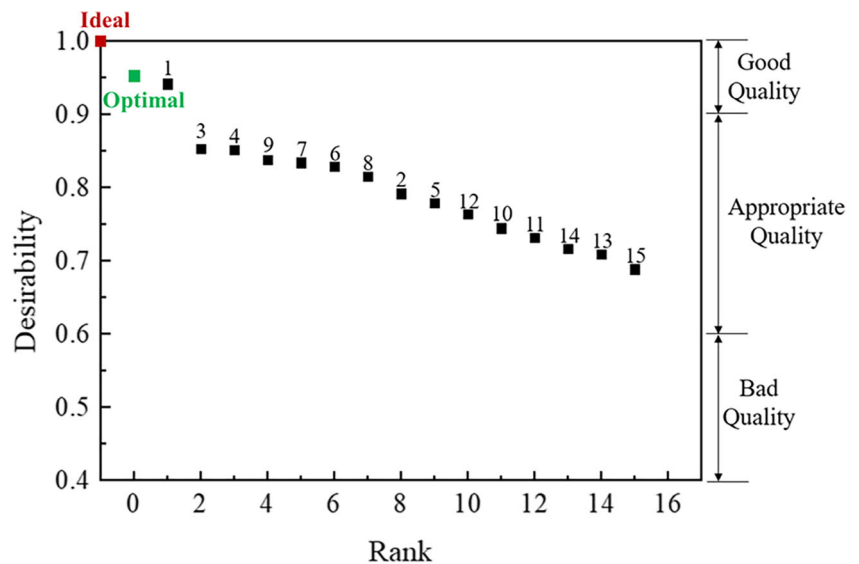

Fig. 8 Thickness profiles of wet coated layer before and after the optimization of the factors

dynamics of ink at the outlet of the slot-die coater and wet coated layer thickness. The application of the model was verified experimentally. Using the model, the thickness profile of the layer in the transverse direction can be obtained according to the geometry of the slot-die coater and coating conditions. The developed model has a superior thickness estimation ability of 92.3%. Based on the developed model, the internal geometry of the slot-die coater and the inlet flow rate were statistically optimized by the Box–Behnken design of the experiment. The optimal factors were determined by using the regression model obtained by ANOVA and the minimum desirability function. Experimental results show that the thickness deviation is improved by 71% in the slot-die coater having the optimal internal geometry and inlet flow rate. We envision that the developed model would be useful to obtain desired coating conditions and the geometry of

Fig. 7 d_m of the ideal ($d_m = 1$) and optimal cases, and experimental results shown in Table 2

the slot-die coater without costly and time-consuming experiments.

References

1. Keränen K, Korhonen P, Rekilä J, Tapaninen O, Happonen T, Makkonen P, Rönkä K (2015) Roll-to-roll printed and assembled large area LED lighting element. Int J Adv Manuf Technol 81:529–536. https://doi.org/10.1007/s00170-015-7244-6

2. Lee J, Kim S, Lee C (2019) Effect of radial stress on the adhesive force of a wound roll in industrial roll-to-roll manufacturing system. Int J Precis Eng Manuf 19(3):411–415. https://doi.org/10.1007/s12541-018-0049-4

3. Park J, Lee J, Park S, Shin K-H, Lee D (2016) Development of hybrid process for double-side flexible printed circuit boards using roll-to-roll gravure printing, via-hole printing, and electroless plating. Int J Adv Manuf Technol 82:9–12. https://doi.org/10.1007/s00170-015-7507-2

4. Lee C (2018) Stresses and defects in roll products: a review of stress models and control techniques. Int J Precis Eng Manuf 19(5):781–789. https://doi.org/10.1007/s12541-018-0094-z

5. Lee J, Kim S, Lee C (2019) Surface drying for brittle material coating without crack defects in large-area roll-to-roll coating system. Int J Precis Eng Manuf Green Tech:1–8. https://doi.org/10.1007/s40684-019-00104-6

6. Park J, Kim S, Lee C (2018) An analysis of pinned edge layer of slot-die coated film in roll-to-roll green manufacturing system. Int J Precis Eng Manuf Green Tech 5(2):247–254. https://doi.org/10.1007/s40684-018-0025-6

7. Romero O, Suszynski W, Scriven L, Carvalho M (2004) Low-flow limit in slot coating of dilute solutions of high molecular weight polymer. J Non-Newtonian Fluid Mech 118(2):137–156. https://doi.org/10.1016/j.jnnfm.2004.03.004

8. Lee J, Nam J (2016) A simple model for viscoplastic thin film formation for coating flows. J Non-Newtonian Fluid Mech 229:16–26. https://doi.org/10.1016/j.jnnfm.2015.12.012

9. Romero O, Scriven L, Carvalho M (2006) Slot-coating of mildly viscoelastic liquids. J Non-Newtonian Fluid Mech 138(2):63–75. https://doi.org/10.1016/j.jnnfm.2005.11.010

10. Chang Y-R, Chang H-M, Lin C-F, Liu T-J, Wu P-Y (2006) Three minimum wet thickness regions of slot die coating. J Colloid Interface Sci 308(1):220–230. https://doi.org/10.1016/j.jcis.2006.11.054

11. Sharma AK, Tiwari AK, Dixit AR (2018) Prediction of temperature distribution over cutting tool with alumina-MWCNT hybrid nanofluid using computational fluid dynamics (CFD) analysis. Int J Adv Manuf Technol 97:427–439. https://doi.org/10.1007/s00170-018-1946-5

12. Park J, Shin K, Lee C (2015) Improvement of cross-machine directional thickness deviation for uniform pressure-sensitive adhesive layer in roll-to-roll slot-die coating process. Int J Precis Eng Manuf 16(5):937–943. https://doi.org/10.1007/s12541-015-0122-1

13. Park J, Shin K, Lee C (2016) Optimized design for anti-reflection coating process in roll-to-roll slot-die coating system. Robot Comput Integr Manuf 30(10):432–441. https://doi.org/10.1016/j.rcim.2014.02.001

14. Hecht DS, Hu L, Irvin G (2011) Emerging transparent electrodes based on thin films of carbon nanotubes, graphene, and metallic nanostructures. Adv Mater 23(13):1482–1513. https://doi.org/10.1002/adma.201003188

15. Shin K, Park J, Lee C (2016) A 250-mm-width, flexible, and continuous roll-to-roll slot-die coated carbon nanotube/silver nanowire film fabrication and a study on the effect of anti-reflective overcoat. Thin Solid Films 598:95–102. https://doi.org/10.1016/j.tsf.2015.12.004

16. Kim S, Kim SY, Chung MH, Kim J, Kim JH (2015) A one-step roll-to-roll process of stable AgNW/PEDOT: PSS solution using imidazole as a mild base for highly conductive and transparent films: optimizations and mechanisms. J Mater Chem C 3(22):5859–5868. https://doi.org/10.1039/C5TC00801H

17. Krebs FC, Fyenbo J, Jørgensen M (2010) Product integration of compact roll-to-roll processed polymer solar cell modules: method and manufacture using flexographic printing, slot-die coating and rotary screen printing. J Mater Chem 20(41):8994–9001 5868. https://doi.org/10.1039/C0JM01178A

18. Schmidt TM, Larsen-Olsen TT, Carlé JE, Angmo D, Krebs FC (2015) Upscaling of perovskite solar cells: fully ambient roll processing of flexible perovskite solar cells with printed back electrodes. Adv Energy Mater 5(15): Paper No. 02164. https://doi.org/10.1002/aenm.201500569

19. Lima FAS, Beliatis MJ, Roth B, Andersen TR, Bortoti A, Reyna Y, Castro E, Vasconcelos IF, Gevorgyan SA, Krebs FC, Lira-Cantu M (2016) Flexible ITO-free organic solar cells applying aqueous solution-processed V2O5 hole transport layer: an outdoor stability study. APL Mater 4(2): Paper No. 1500569. https://doi.org/10.1063/1.4942638

20. Helgesen M, Carle JE, Krebs FC (2013) Slot-die coating of a high performance copolymer in a readily scalable roll process for polymer solar cells. Adv Energy Mater 3(12):1664–1669. https://doi.org/10.1002/aenm.201300324

21. Sandström A, Dam HF, Krebs FC, Edman L (2012) Ambient fabrication of flexible and large-area organic light-emitting devices using slot-die coating. Nat Commun 3(1002). https://doi.org/10.1038/ncomms2002

22. Lee J, Kim S, Lee C (2019) Large area electrolyte coating through surface and interface engineering in roll-to-roll slot-die coating process. J Ind Eng Chem 76(25):443–449. https://doi.org/10.1016/j.jiec.2019.04.011

23. Lee J, Park J, Jeong H, Shin K, Lee D (2016) Optimization of printing conditions for microscale multiline printing in continuous roll-to-roll gravure printing. J Ind Eng Chem 42(10):131–141. https://doi.org/10.1016/j.jiec.2016.07.031

24. Lee C, Kang H, Kim C, Shin K (2010) A novel method to guarantee the specified thickness and surface roughness of the roll-to-roll printed patterns using the tension of a moving substrate. J Microelectromech 19(5):1243–1253. https://doi.org/10.1109/JMEMS.2010.2067194